A Fast and General Method to Calculate Mutual Inductance for EV Dynamic Wireless Charging System

Beibei Song, Shumei Cui, Yong Li, and Chunbo Zhu, *Member, IEEE*

***Abstract*—For the electric vehicle (EV) dynamic wireless charging system, mutual inductance is an important factor affecting the output power. In this article, a fast and general method to calculate mutual inductance is proposed. This method can calculate the mutual inductance of magnetic couplers with different receiver structures and receiver positons by only one simulation, and it can also provide a theoretical guidance for the receiver design. Calculation models for different receiver structures are established, and the mutual inductance calculation-coefficients are proposed to describe the functional relationships between mutual inductance and receiver's parameters. Based on the concept of mutual inductance calculation-coefficients, the surface-integral in the conventional analytical calculation method can be simplified to be the product of these coefficients and magnetic flux density's amplitude, and then the calculation difficulty of the mutual inductance can be reduced. Finally, a prototype was built for experimental verification. The experiment results show that the max error between the measured mutual inductance and the calculated result is only 1.56%, which verifies the feasibility and the accuracy of the proposed calculation method.**

***Index Terms*—Calculation method, dynamic wireless charging (DWC) system, EV, mutual inductance, mutual inductance calculation coefficients.**

I. Introduction

DYNAMIC wireless charging (DWC) technology can realize the nonstop charging for EVs, effectively increase the cruising range of vehicles, and reduce the waiting time of parking charging [1]–[4]. In the DWC system, the power supply rail is buried under the ground, and it cannot be modified after construction. Since different types of vehicles (cars, buses, etc.) have different requirements on output voltage and output power, the on-board receivers should be designed independently to ensure the applicability of different vehicles to common power supply rail. As the most important factor that directly determines the output power, mutual inductance is related to many parameters such as the position and structure of the receiver [5]–[8]. Therefore, the calculation of mutual inductance and the relationship between mutual inductance and the receiver's parameters are the key points in the receiver design process.

At present, there are three mainstream methods to calculate mutual inductance, and the first one is analytical calculation method. The basic idea of this method is to integrate the magnetic flux density passing through the coil. For static wireless charging systems, the analytical methods to calculate the mutual inductance of planar-circular coils were proposed in [9]–[13], two calculation methods for coaxial coils were proposed in [10] and [14], and the calculation methods for rectangular coil with or without aluminum shield were proposed in [15] and [16], respectively. For the DWC system, a calculation method for coreless power supply rail was proposed in [17]. However, the earlier analytical methods are only suitable for the magnetic couplers without core or with simple core structure. When the structure of the ferrite core or of the coil is complex, the distribution of magnetic field is difficult to be described by equation, which makes the mutual inductance difficult to be calculated analytically.

The second method, to calculate mutual inductance, is the simulation method. This method uses software such as Ansoft to obtain the mutual inductance. Since this method is suitable for the magnetic coupler with complex core structures, it is widely used in DWC systems [18]–[21]. Based on this method, the effect of the receiver's structural parameters on the mutual inductance can also be analyzed by parameters sweeping [22]–[25]. However, the main disadvantage of this method is that the simulation model required to be resimulated when the structure or the position of the receiver is changed. During the receiver design and optimization process, this method usually requires thousands of simulations to derive the relationship between the mutual inductance and the receiver's structural parameters, which is very time consuming, especially for the cases when three-dimensional simulations are required.

The third calculation method is only suitable for the power supply rails with alternately arranged poles. The mutual inductance of the magnetic couplers with I-type and S-type rails was respectively calculated by this method [26], [27]. In this method, the structure of the receiver is determined first, and then the effective area-coefficient is obtained by finite-element simulations. Finally, the mutual inductance can be calculated by the product of the magnetic flux density's amplitude and the

Manuscript received February 11, 2020; revised June 21, 2020; accepted July 31, 2020. Date of publication August 7, 2020; date of current version October 30, 2020. This work was supported by National Basic Enhancement Program of China under Grant 2019-JCJQ-JJ-316. Recommended for publication by Associate Editor O. C. Onar. *(Corresponding author: Shumei Cui.)*

The authors are with the School of Electrical Engineering & Automation, Harbin Institute of Technology, Harbin 150001, China (e-mail: songbei_mt@126.com; cuism@hit.edu.cn; liyong611@hit.edu.cn; zhuchunbo@hit.edu.cn).

Color versions of one or more of the figures in this article are available online at https://ieeexplore.ieee.org.

Digital Object Identifier 10.1109/TPEL.2020.3015100

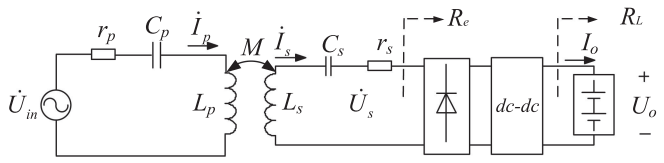

Fig. 1. Equivalent circuit of the DWC system.

effective area-coefficient. However, this method requires lots of finite-element simulations to obtain the effective area coefficient. Moreover, when the structure of the receiver is changed, the simulations need to be repeated to derive the new effective area-coefficient.

In summary, the analytical method has the disadvantage of narrow applicability and it cannot be applied to the DWC system with complex core or coil structure. While the simulation method and the third method need to rebuild the model for simulation when the receiver is changed. Moreover, all the earlier methods cannot provide the functional relationship between mutual inductance and receiver's parameters, which results in the lack of the receiver's design principle.

Considering the gaps of the existing research, the purpose of this article is to propose a fast and general method to calculate the mutual inductance. In this method, mutual inductance calculation-coefficients are proposed to describe the functional relationship between mutual inductance and receiver's parameters. Then, the mutual inductance can be calculated by the product of the calculation-coefficients and magnetic flux density's amplitude. Compared with the simulation calculation method, the proposed method can calculate the mutual inductance of the magnetic couplers with different receiver structures by only one simulation.

The remaining of the article is organized as follows. By taking the power supply rails with alternately arranged poles as an example, Section II demonstrates how to calculate the mutual inductance by the proposed calculation-coefficients. Section III gives the physical meaning and calculation method of the mutual inductance calculation-coefficients. In Section IV, the feasibility and the accuracy of the proposed calculation method are verified by simulation and experiments. In Section V, the conclusion is drawn.

II. Calculation Method of Mutual Inductance

A. Effect of Mutual Inductance on the DWC System

When the series-series (SS) compensation network is applied to the DWC system, the equivalent circuit of the system is shown in Fig. 1 .

In the earlier figure, M indicates the mutual inductance between the transmitter and receiver coils, r_p and L_p indicate the internal resistance and self-inductance of the transmitter coil, respectively, and C_p and I_p, indicate the resonant capacitor and the current in the transmitter coil, respectively. Similarly, the corresponding parameters of the receiver are, respectively, indicated as r_s, L_s, C_s, and I_s. In addition, Re indicates the

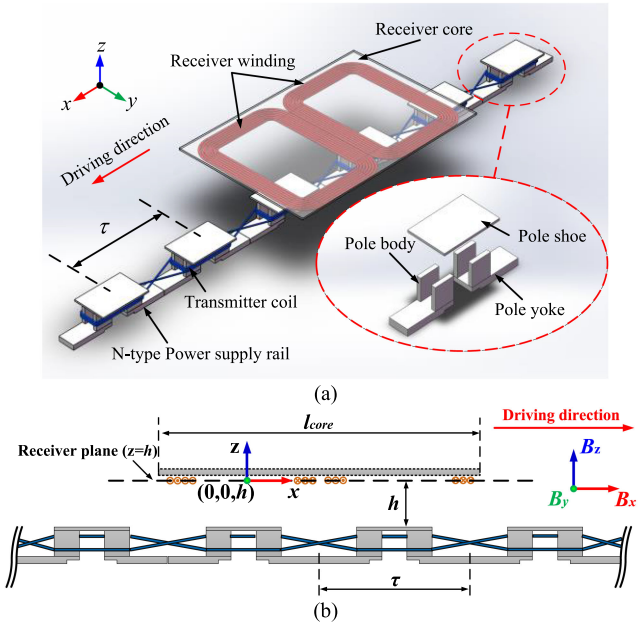

Fig. 2. Structure diagrams of the magnetic coupler used in the DWC system. (a) Bird view. (b) Main view.

impedance of the battery load from the dc/dc converter and the rectifier to the receiver coil port.

Based on the equivalent circuit shown in Fig. 1, the output power of the system (denoted as P_{out}) can be calculated by

$$P_{\text{out}} = \frac{U^2{}_{\text{oc}}}{(R_e + r_s)^2} \cdot R_e \tag{1}$$

where U_{oc} indicates the open-circuit voltage of the receiver coil.

According to the theory of electromagnetic induction, U_{oc} is generated by the mutual flux linkage passing through the receiver coil (denoted as ψ_{m}), and it can be expressed as [28]

$$U_{\text{oc}} = \frac{d\psi_m}{dt} = \omega \cdot M \cdot I_P. \tag{2}$$

Substituting (2) into (1), P_{out} can be expressed as

$$P_{\text{out}} = \frac{\omega^2 \cdot M^2 \cdot I_p^2}{(R_e + r_s)^2} \cdot R_e. \tag{3}$$

It can be seen from (3) that P_{out} is proportional to the square of M. When Re is fixed, the output power can be improved by increasing the mutual inductance. As an important factor affecting the output power, when the structure of the power supply rail is fixed, mutual inductance is determined by the parameters of the receiver. Therefore, in the receiver design phase, it is necessary to calculate the mutual inductance and analyze the effects of the receiver's parameters on the mutual inductance. At this time, the reasonable structural parameters of the receiver can be designed [22]–[27].

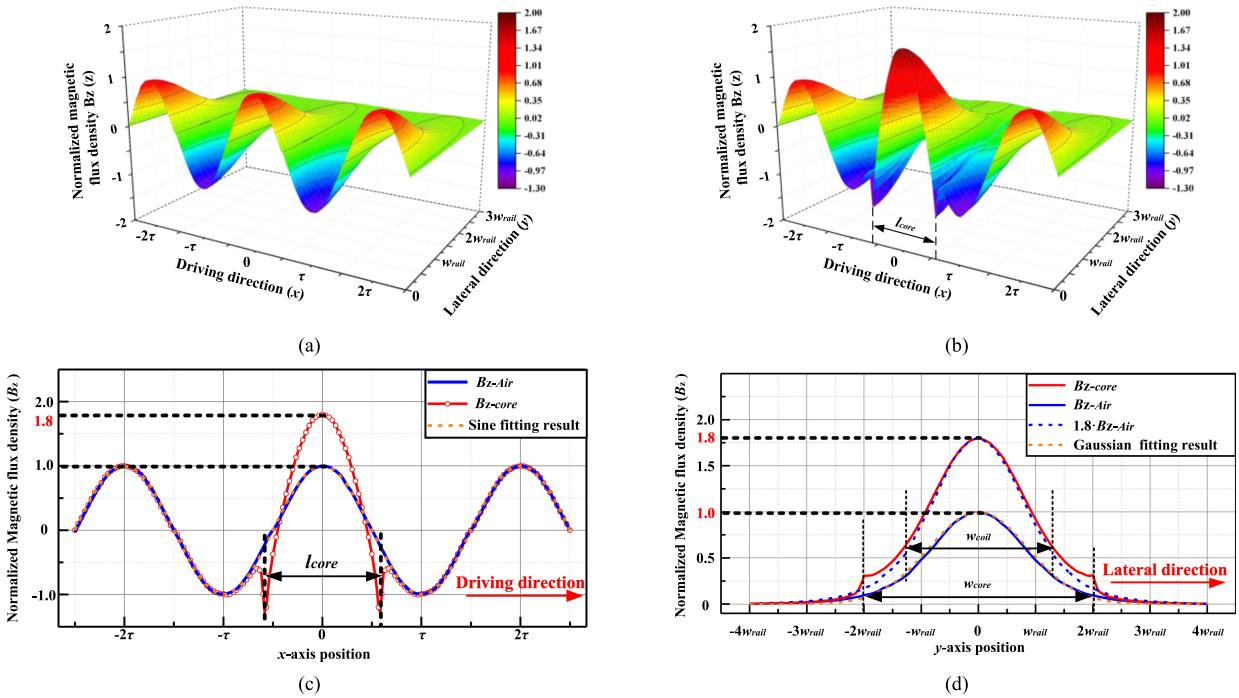

Fig. 3. The normalized simulation results of B_z. (a) Distribution of B_z without receiver core. (b) Distribution of B_z with a plate receiver core. (c) Distribution of B_z on the straight line $y = 0$. (d) Distribution of B_z on the straight line $x = 0$.

B. Magnetic Field Distribution of the Magnetic Coupler

The magnetic coupler used in the DWC system is shown in Fig. 2(a). It consists of two parts: an on-board receiver, and an N-type power supply rail. The power supply rail is buried under the ground, it consists of a transmitter coil and a rail core. According to the different roles, the rail core can be divided into three parts: a pole body, a pole shoe and a pole yoke.

Before calculating the mutual inductance, the distribution of the magnetic field generated by the power supply rail should be analyzed first. As shown in Fig. 2(b), the magnetic field on the receiver plane ($z = h$) can be decomposed into three components along the x-axis, y-axis, and z-axis (denoted as B_x, B_y and B_z), respectively. Since the directions of B_x and B_y are parallel to the receiver plane, B_x and B_y have no effect on the mutual flux linkage passing through the receiver coil.

For the magnetic coupler without receiver core, the normalized simulation result of B_z (denoted as $B_{z-\mathrm{Air}}$) on receiver plane is shown in Fig. 3(a). Since the distribution of $B_{z-\mathrm{Air}}$ is symmetrical about the x-axis, only the distribution when $y \geqslant 0$ is shown in the figure. The distributions of $B_{z-\mathrm{Air}}$ on straight lines $x = 0$ and $y = 0$ are, respectively, shown in Fig. 3(c) and (d) by the blue curves.

As shown in Fig. 3(c), the distribution of $B_{z-\mathrm{Air}}$ along the driving direction (x-axis) is a sine function with a period of 2τ. On the straight line $y = 0$, $B_{z-\mathrm{Air}}$ can be expressed as

$$B_{z-\mathrm{Air}}(x,0) = B_z(0,0) \cdot \cos\left(\frac{x}{\tau} \cdot 180^\circ\right) = B_{z-\max} \cdot \cos\left(\frac{x}{\tau} \cdot 180^\circ\right) \quad (4)$$

where $B_{z-\max}$ indicates the peak value of $B_{z-\mathrm{Air}}$ and is equal to the value of $B_{z-\mathrm{Air}}$ at point (0,0).

As shown in Fig. 3(d), the distribution of $B_{z-\mathrm{Air}}$ along the lateral direction (y-axis) is a Gaussian function. Therefore, on the straight line $x = 0$, $B_{z-\mathrm{Air}}$ can be expressed as:

$$B_{z-\mathrm{Air}}(0,y) = B_z(0,0) \cdot e^{\frac{-y^2}{2\sigma^2}} = B_{z-\max} \cdot e^{\frac{-y^2}{2\sigma^2}} \quad (5)$$

where σ is called shape-parameter, it affects the shape of the Gaussian curve, and it is determined by the structure of the power supply rail and the air gap of the magnetic coupler.

As shown in Fig. 3(a), on any straight line ($x = x_0$) parallel to the y-axis, the distribution of $B_{z-\mathrm{Air}}$ along the y-direction is also a Gaussian function. Therefore, on the straight line $x = x_0$, $B_{z-\mathrm{Air}}$ can be expressed as

$$B_{z-\mathrm{Air}}(x_0,y) = B_z(x_0,0) \cdot e^{\frac{-y^2}{2\sigma^2}}. \quad (6)$$

Substituting (4) into (6), the expression of $B_{z-\mathrm{Air}}$ at any point (x_0, y_0) on the receiver plane can be obtained as

$$B_{z-\mathrm{Air}}(x_0,y_0) = B_z(x_0,0) \cdot e^{\frac{-y_0^2}{2\sigma^2}} = B_{z-\max} \cdot \cos\left(\frac{x_0}{\tau} \cdot 180^\circ\right) \cdot e^{\frac{-y_0^2}{2\sigma^2}}. \quad (7)$$

Therefore, for the magnetic coupler without receiver core, the magnetic density component $B_{z-\mathrm{Air}}$ on the receiver plane can be expressed as follows:

$$B_{z-\mathrm{Air}}(x,y) = B_{z-\max} \cdot \cos\left(\frac{x}{\tau} \cdot 180^\circ\right) \cdot e^{\frac{-y^2}{2\sigma^2}}. \quad (8)$$

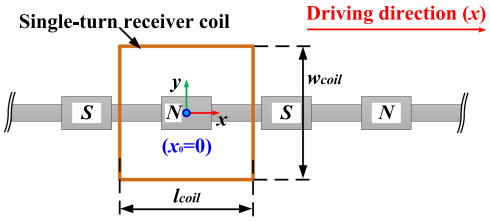

Fig. 4. Structure diagram of the magnetic coupler with single-turn receiver coil.

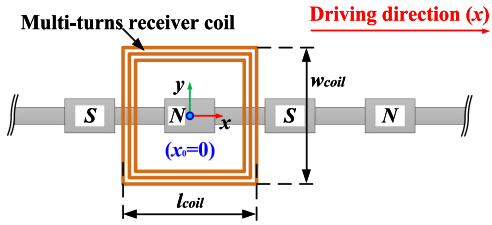

Fig. 5. Structure diagram of the magnetic coupler with multi-turns receiver coil.

For the magnetic coupler with a plate receiver core, the normalized simulation result of B_z (denoted as $B_{z-\mathrm{core}}$) on receiver plane is shown in Fig. 3(b). The distributions of $B_{z-\mathrm{core}}$ on straight lines $x = 0$ and $y = 0$ are shown in Fig. 3(c) and (d) by the red curves, respectively.

It can be seen from Fig. 3(b)–(d) that are as follows.

1) In the region beyond the receiver core, the plate receiver core has no effect on the distribution of B_z.
2) In the region directly below the receiver core, B_z increases k_c times, where k_c is affected by the size of the receiver core and is equal to 1.8 in Fig. 3;
3) In the region below the edge of the receiver core, B_z has a small distortion due to the end effect of the receiver core.

Therefore, when the receiver coil is arranged directly below the receiver core, the magnetic density component $B_{z-\mathrm{core}}$ passing through the receiver coil is k_c times that of $B_{z-\mathrm{Air}}$. As a result, $B_{z-\mathrm{core}}$ can be expressed as

$$\begin{aligned} B_{z-\mathrm{Core}}(x,y) &= k_c \cdot B_{z-\mathrm{Air}}(x,y) \\ &= k_c \cdot B_{z-\max} \cdot \cos\left(\frac{x}{\tau}\cdot 180^\circ\right) \cdot e^{\frac{-y^2}{2\sigma^2}}. \end{aligned} \tag{9}$$

C. Calculation Modeling of Mutual Inductance

Mutual inductance is defined as

$$M = \frac{\psi_m}{I_p} \tag{10}$$

where ψ_m is the mutual flux linkage in the receiver coil and I_p is the transmitter current.

When the structure of power supply rail and the air gap are fixed, mutual inductance is only determined by the receiver's structure and position.

1) Receiver Coil With Single-Turn: For the receiver with single-turn receiver coil, the structure diagram of the magnetic coupler is shown in Fig. 4. As shown in the figure, the coil length is l_{coil} and the coil width is w_{coil}. The mutual flux linkage passing through the receiver coil can be calculated by

$$\psi_m = \int\int_S B_z(x,y)ds = \int_{\frac{-w_{\mathrm{coil}}}{2}}^{\frac{w_{\mathrm{coil}}}{2}} \int_{\frac{-l_{\mathrm{coil}}}{2}+x_0}^{\frac{l_{\mathrm{coil}}}{2}+x_0} B_z(x,y)dxdy \tag{11}$$

where x_0 indicates the positon of the receiver.

By substituting (8) into 11), we can get that

$$\psi_m = \int_{\frac{-w_{\mathrm{coil}}}{2}}^{\frac{w_{\mathrm{coil}}}{2}} \int_{\frac{-l_{\mathrm{coil}}}{2}+x_0}^{\frac{l_{\mathrm{coil}}}{2}+x_0} B_{z-\max}\cdot\cos\left(\frac{x}{\tau}\cdot\pi\right)\cdot e^{\frac{-y^2}{2\sigma^2}}dxdy$$

$$\begin{aligned} &= \frac{2\tau}{\pi}\cdot B_{z-\max}\cdot\cos\left(\frac{\pi}{\tau}\cdot x_0\right)\cdot\sin\left(\frac{l_{\mathrm{coil}}}{\tau}\cdot\frac{\pi}{2}\right) \\ &\quad\cdot\int_{\frac{-w_{\mathrm{coil}}}{2}}^{\frac{w_{\mathrm{coil}}}{2}} e^{\frac{-y^2}{2\sigma^2}}dy \\ &= \frac{2\tau}{\pi}\cdot B_{z-\max}\cdot k_x\cdot k_l\cdot k_w \end{aligned} \tag{12}$$

where

$$k_x = \cos\left(\frac{\pi}{\tau}\cdot x_0\right) \tag{13}$$

$$k_l = \sin\left(\frac{l_{\mathrm{coil}}}{\tau}\cdot\frac{\pi}{2}\right) \tag{14}$$

$$k_w = \int_{\frac{-w_{\mathrm{coil}}}{2}}^{\frac{w_{\mathrm{coil}}}{2}} e^{\frac{-y^2}{2\sigma^2}}dy. \tag{15}$$

In the earlier equations, k_x, k_l, and k_w are defined as position-coefficient, length-coefficient and width-coefficient, respectively. These coefficients can describe the functional relationships between mutual inductance and the position of the receiver, the length of the receiver coil and the width of the receiver coil, respectively.

According to (12), the effect of receiver's position x, receiver coil's length l_{coil} and receiver coil's width w_{coil} on the mutual flux linkage is independent. Therefore, when the size of the receiver coil is fixed, mutual inductance is only determined by the position of the receiver.

2) Receiver Coil With Multiturns: For the receiver coil with N_S turns, the structure diagram of the magnetic coupler is shown in Fig. 5.

At this time, the total mutual flux linkage passing thorough the receiver coil (denoted as $\psi_{m\text{-}\Sigma}$) is the sum of the mutual flux linkages passing through each turn of the coil. $\psi_{m\text{-}\Sigma}$ can be expressed as

$$\psi_{m-\Sigma} = \sum_{i=1}^{N_S}\psi_{m-i}. \tag{16}$$

Due to the wire diameter, the sizes of the inside turn and the outside turn are quite different, which makes the mutual inductance no longer simply proportional to the number of turns. Therefore, the concept of turns-coefficient (denoted as k_N) is proposed. By this coefficient, the total mutual flux linkage $\psi_{m\text{-}\Sigma}$ can be regarded as the product of the number of turns N_S and the flux linkage passing through the outermost turn (denoted

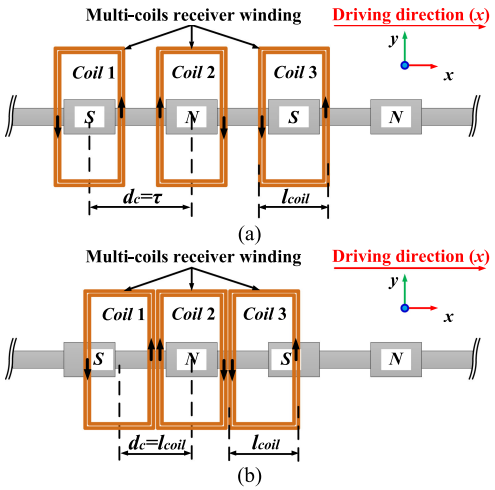

Fig. 6. Structure diagram of the magnetic coupler with multicoils. (a) $d_c = \tau$. (b) $d_c \neq \tau$.

as $\psi_{m\text{-}1}$). And k_N can be expressed as follows:

$$k_N = \frac{\sum_{i=1}^{N_S} \psi_{m-i}}{N_S \cdot \psi_{m-1}}. \tag{17}$$

In summary, for the receiver coil with multi-turns, the expression of the mutual flux linkage can be rewritten as

$$\begin{aligned} \psi_{m-\Sigma} &= N_S \cdot k_N \cdot \psi_{m-1} \\ &= \frac{2\tau}{\pi} \cdot B_{z-max} \cdot k_x \cdot k_l \cdot k_w \cdot (N_S \cdot k_N). \end{aligned} \tag{18}$$

3) Receiver With Multicoils: When the output voltage of a single receiver coil cannot meet the output requirement, the receiver with multicoils connected in series is usually used to increase output voltage.

Fig. 6(a) shows the structure diagram of the magnetic coupler when the center distance between the receiver coils (denoted as d_c) is equal to the pole distance τ. In order to obtain the maximum mutual flux linkage passing through the receiver coils, each two adjacent receiver coils are wound in opposite direction. As shown in Fig. 6(a), when a single receiver coil moves to the position directly above a magnetic pole, the other receiver coils will also be directly above the other poles. Therefore, during the driving process of the vehicle, the mutual flux linkages passing through each receiver coil (denoted as $\psi_{m\text{-coil1}}$, $\psi_{m\text{-coil2}}$, and $\psi_{m\text{-coil3}}$) are equal at any positon. And the total flux linkage passing through all the coils is equal to the product of the number of coils (denoted as q) and the flux linkage passing through a single coil.

Fig. 6(b) shows the structure diagram of the magnetic coupler when d_c is not equal τ. At this time, $\psi_{m\text{-coil1}}$, $\psi_{m\text{-coil2}}$, and $\psi_{m\text{-coil3}}$ are no longer the same, but have a phase difference along the driving direction. As shown in Fig. 7, during the driving process of EV, $\psi_{m\text{-coil1}}$, $\psi_{m\text{-coil2}}$, and $\psi_{m\text{-coil3}}$ vary sinusoidally with the position of the receiver x, and the phase differences between $\psi_{m\text{-coil1}}$, $\psi_{m\text{-coil2}}$, and $\psi_{m\text{-coil3}}$ are always fixed at a constant value.

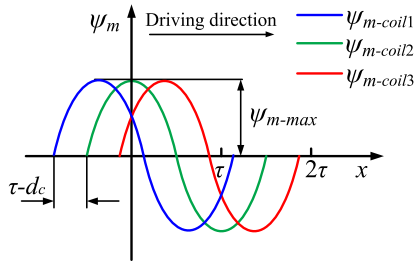

Fig. 7. The mutual flux linkages passing through each receiver coil versus the position of the receiver x.

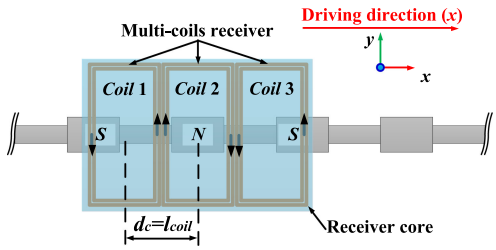

Fig. 8. Structure diagram of the magnetic coupler with a plate receiver core.

Therefore, the total mutual flux linkage passing through all the receiver coils cannot be simply calculated by the number of coils q. To solve this problem, the distance-coefficient (denoted as k_d) is proposed to describe the functional relationship between the mutual flux linkage and the center distance of receiver coils.

Based on the distance-coefficient, for the receiver with multi-coils, the expression of the mutual flux linkage can be rewritten as follows:

$$\psi_m = \frac{2\tau}{\pi} \cdot B_{z-\max} \cdot k_x \cdot k_l \cdot k_w \cdot (N_S \cdot k_N) \cdot q \cdot k_d. \tag{19}$$

4) Receiver With Plate Core: Plate receiver core is widely used in the DWC system for EV. Fig. 8 shows the structure diagram of the magnetic coupler with a plate receiver core.

According to (8) and (9), after using the plate receiver core, the magnetic field component B_z passing through the receiver coil is increased to k_c times of that without core. At this time, the expression of the mutual flux linkage can be rewritten as follows:

$$\psi_m = \frac{2\tau}{\pi} \cdot B_{z-\max} \cdot k_x \cdot k_l \cdot k_w \cdot (N_S \cdot k_N) \cdot q \cdot k_d \cdot k_c \tag{20}$$

where k_c is defined as core-coefficient, it is used to describe the amplification factor of the mutual inductance after using a plate receiver core.

D. General Calculation Method of Mutual Inductance

Based on the calculation models established earlier, a general method to calculate mutual inductance is proposed, as shown in Fig. 9. The mutual inductance of the magnetic couplers with different receiver structures and receiver positions can be

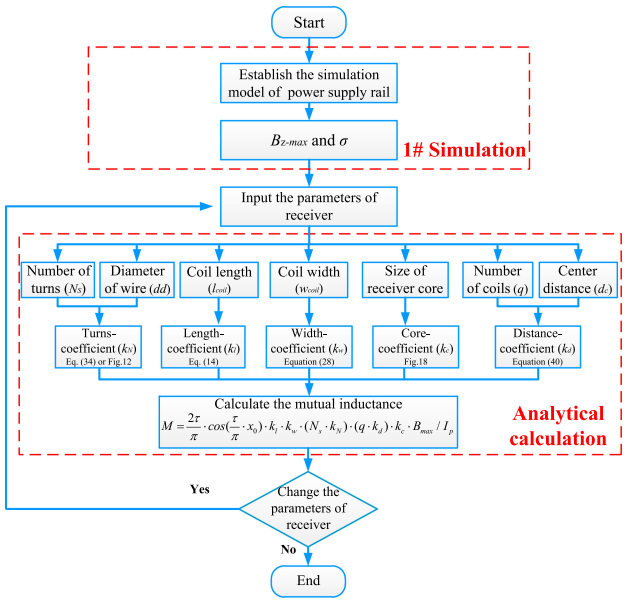

Fig. 9. Proposed calculation method of mutual inductance.

calculated directly by the following equation:

$$M=\frac{\psi_m}{I_p}=\frac{2\tau}{\pi}\cdot\frac{B_{z-\max}}{I_p}\cdot k_x\cdot k_l\cdot k_w\cdot N_S\cdot k_N\cdot q\cdot k_d\cdot k_c. \tag{21}$$

The basic idea of the propose method is to use different calculation-coefficients to describe the functional relationships between mutual inductance and the receiver's parameters (such as the size, the number of turns and the positon of the receiver coil, etc.). Then the calculation of the mutual inductance can be simplified from the magnetic flux's integral in the conventional analytical method to the product of the coefficients and $B_{z-\max}$. In this way, the calculation difficulty can be reduced and the calculation speed can be increased. The calculation method of each coefficient will be illustrated in Section III in detail.

The steps of the proposed method can be summarized as follows:

1) obtain the magnetic density amplitude $B_{z-\max}$ and the shape-parameter σ by only one simulation;
2) determine the value of each calculation-coefficient according to the receiver's parameters;
3) calculate the mutual inductance value by (21).

During the receiver design and optimization process, the conventional design method adopts finite-element simulations to design the structural parameters of receiver. Based on the proposed calculation method, sweeping parameters in simulations can be replaced by changing the values of the calculation coefficients. Therefore, thousands of simulations can be eliminated and the design time can be greatly reduced.

E. Calculation Time

The calculation time of the proposed method can be divided into two parts. The first part is the time for single finite element simulation. For a computer with 64G memory, the time required for a single simulation is about 5 min. Since the proposed method only requires one simulation, the calculation time of the first part is 5 min.

The second part is the time for analytical calculation. After inputting the equations of each calculation-coefficients (k_l, k_w and so on) into Matlab, the mutual inductance of the magnetic coupler with different receiver parameters can be calculated rapidly by entering the receiver's parameters. For a computer with 64G memory, the calculation time of the second part is within 1 min. Therefore, the total calculation time of the proposed method is

$$t_{\text{proposed}}=5\text{ min}+1\text{ min}=6\text{ min}. \tag{22}$$

Due to the large air gap between the receiver and the power supply rail, the mutual inductance is calculated by finite-element simulation in the conventional calculation method. Fig. 10 shows the steps of the conventional method.

In the conventional method, the relationship between the mutual inductance and the receiver's parameters is obtained by sweeping the parameters in the finite-element simulations.

Assuming that each parameter of the receiver required to be swept N times in the simulation. For example, in order to obtain the relationship between the mutual inductance and the five structural parameters of the receiver coil (l_{coil}, w_{coil}, N_S, d_c and q), N^5 simulations are required.

Since eight simulations can be conducted simultaneously in a computer with eight-cores, the average time required for a single simulation is

$$t_{\text{FEM}-1}=\frac{5\text{ min}}{8}=0.625\text{ min}. \tag{23}$$

Assuming that $N=5$, the calculation time of the conventional method (denoted as t_{FEM}) is

$$t_{\text{FEM}}=N^5\cdot 0.625\text{ min}=1953.125\text{ min}\approx 162.8\text{ h}. \tag{24}$$

According to (22) and (24), the calculation time of the proposed method is far less than that of the conventional FEM method. Moreover, as N and the number of the parameters

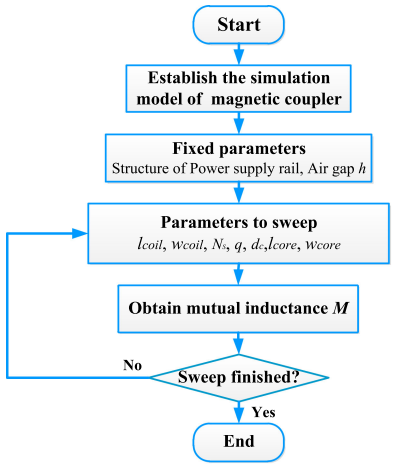

Fig. 10. Conventional FEM method to calculate mutual inductance.

required to be swept increase, the advantage of the proposed method in computing speed is much more obvious than that of the conventional method.

III. Calculation Method of Each Calculation-Coefficient

The mutual inductance calculation-coefficients proposed in this paper reveal the intrinsic relationship between mutual inductance and each parameter of the receiver. Besides calculating mutual inductance, the calculation-coefficients can also give the selection principle of the receiver's parameters and provide a theoretical guidance for the receiver structure design. This section illustrates the calculation method of each calculation-coefficient in detail.

A. Position-Coefficient and Length-Coefficient

The position-coefficient and the length-coefficient can be calculated by (13) and (14), respectively.

It can be seen from (14) that the mutual inductance *M* varies sinusoidally with the length of the receiver coil l_{coil}. When l_{coil} is equal to the pole pitch τ, k_l reaches the maximum value. At this time, the magnetic coupler has the maximum mutual inductance.

The length-coefficient k_l can provide a theoretical guidance for the design of the receiver coil length. Based on the relationship between l_{coil} and τ, the receiver coil can be divided into short-pitch coil ($l_{\mathrm{coil}} < \tau$), full-pitch coil ($l_{\mathrm{coil}} = \tau$), and long-pitch coil ($l_{\mathrm{coil}} > \tau$). When the width of the receiver coil is fixed, according to (14), the mutual inductance of the short-pitch coil and the long-pitch coil is smaller than that of the full-pitch coil.

Therefore, in order to improve the output power, full-pitch receiver coil is usually adopted in the receiver design process to maximize the mutual inductance. However, when the size of the vehicle chassis is limited, the on-board receiver shall adopt short-pitch coil to meet the requirement of installation space at the expense of mutual inductance. Compared with full-pitch receiver coil, long-pitch coil has the disadvantages of small mutual inductance, high cost and large installation space. Adopting long-pitch coil as the receiver coil not only wastes the materials, but also reduces the coupling coefficient and the efficiency of the system. Therefore, long-pitch receiver coil shall only be used in some special application background.

B. Width-Coefficient

The width-coefficient k_w can describe the functional relationship between the mutual inductance and the width of the receiver coil. According to (15), the calculation of the width coefficient requires integral of B_z along the *y*-axis, where the upper and lower limits of the integral are determined by the width of the receiver coil. Since the distribution of B_z along the *y*-axis is a Gaussian function, the calculation of k_w can be simplified from an integral problem to a probability calculation problem by using the theory of normal distribution.

Based on this idea, (15) can be rewritten as

$$k_w = \int_{\frac{-w_{\mathrm{coil}}}{2}}^{\frac{w_{\mathrm{coil}}}{2}} e^{\frac{-y^2}{2\sigma^2}}\,dy = \sqrt{2\pi}\cdot\sigma\int_{\frac{-w_{\mathrm{coil}}}{2}}^{\frac{w_{\mathrm{coil}}}{2}} \frac{1}{\sqrt{2\pi}\cdot\sigma} e^{\frac{-y^2}{2\sigma^2}}\,dy. \tag{25}$$

As can be seen from the above equation, the width coefficient k_w follows a normal distribution, that is, $k_w \sim N(0, \sigma^2)$. According to the theory of normal distribution, the distribution function of k_w can be expressed as

$$F(y) = \frac{1}{\sqrt{2\pi}\cdot\sigma}\cdot\int_{-\infty}^{y} e^{\frac{-t^2}{2\sigma^2}}\,dt. \tag{26}$$

The distribution function is used to simplify the integral problem of the Gaussian function. By using the distribution function, the integral part of (25) can be simplified to

$$\begin{aligned}\int_{\frac{-w_{\mathrm{coil}}}{2}}^{\frac{w_{\mathrm{coil}}}{2}} \frac{1}{\sqrt{2\pi}\cdot\sigma}\cdot e^{\frac{-y^2}{2\sigma^2}}\,dy &= 2F\left(\frac{w_{\mathrm{coil}}}{2}\right) - 1 \\ &= 2\Phi\left(\frac{w_{\mathrm{coil}}}{2\sigma}\right) - 1\end{aligned} \tag{27}$$

where $\Phi(x)$ is the distribution function of the standard normal distribution, and it can be obtained from the standard normal distribution table.

By substituting (27) into (25), the width-coefficient k_w can be expressed as follows:

$$k_w = \sqrt{2\pi}\cdot\sigma\cdot\left[2\Phi\left(\frac{w_{\mathrm{coil}}}{2\sigma}\right) - 1\right]. \tag{28}$$

Based on the normal distribution theory, the integral problem of the width-coefficient's calculation can be simplified to the problem of calculating the probability $P(-0.5w_{\mathrm{coil}} \le k_w \le 0.5w_{\mathrm{coil}})$. And according to the expression of k_w, the mutual inductance of the magnetic coupler with different receiver coil width can be calculated by only changing the value of w_{coil} in (28).

The width-coefficient k_w can also provide a theoretical guidance for the receiver design. Since k_w follows the standard normal distribution, the 3σ criterion can be extended to the receiver design process. According to the 3σ criterion, $k_w(w_{\mathrm{coil}} = 4\sigma) = 0.9544$, $k_w(w_{\mathrm{coil}} = 6\sigma) = 0.9974$, and $k_w(w_{\mathrm{coil}} = +\infty) = 1$. When w_{coil} exceeds 6σ, further increasing the width of the receiver coil can only increase k_w from 0.9974 to 1. Since the mutual inductance is proportional to k_w, when w_{coil} exceeds 6σ, increasing the width of the receiver coil has little improvement on the mutual inductance (less than 0.3%). At this time, the coupling coefficient *k* will decrease with the increase of w_{coil}, resulting in a drop of the system efficiency.

In summary, in the receiver design process, the width of the receiver coil should satisfies that $w_{\mathrm{coil}} \le 6\sigma$.

C. Turns-Coefficient

The turns-coefficient k_N can describe the functional relationship between mutual inductance and the number of turns of the receiver coil. The structure diagram of the receiver coil with N_S turns is shown in Fig. 11, and the distance between two adjacent turns is denoted as *dd*. For the convenience of description, subscripts are used to number each turn of the receiver coils,

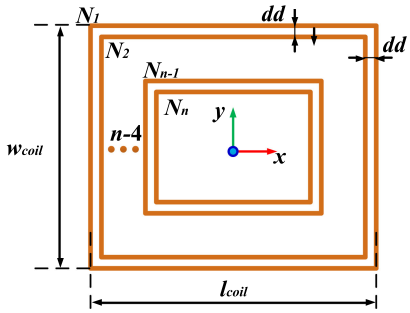

Fig. 11. Structure diagram of the receiver coil with multi-turns.

where subscript 1 represents the outermost coil and subscript *S* represents the innermost coil.

For the *i*th turn of the coil (denoted as N_i), the coil length is l_{coil}-2*(i-1)·dd*, and the coil width is w_{coil}-2*(i-1)·dd*. Substituting them into (14) and (28), the length-coefficient (denoted as k_{l-i}) and the width-coefficient (denoted as k_{w-i}) of N_i can be obtained as follows:

$$k_{l-i} = \sin\left(\frac{l_{\text{coil}} - 2(i-1)\cdot dd}{\tau}\cdot\frac{\pi}{2}\right) \tag{29}$$

$$k_{w-i} = \sqrt{2\pi}\cdot\sigma\cdot\left[2\Phi\left(\frac{w_{\text{coil}} - 2(i-1)\cdot dd}{2\sigma}\right) - 1\right]. \tag{30}$$

Then, the total mutual flux linkage passing through all the turns of the coil can be expressed as

$$\psi_{m-\Sigma} = \frac{2\tau}{\pi}\cdot B_{z-\max}\cdot k_x\cdot\sum_{i=1}^{N_S}(k_{l-i}\cdot k_{w-i}). \tag{31}$$

Since the outermost turn determines the overall dimensions of the receiver coil, $k_{l\text{-}1}$ and $k_{w\text{-}1}$ satisfy that

$$k_l = k_{l-1}, k_w = k_{w-1}. \tag{32}$$

Therefore, the mutual flux linkage passing through the outermost turn (denoted as $\psi_{m\text{-}1}$) can be expressed as

$$\psi_{m-1} = \frac{2\tau}{\pi}\cdot B_{z-\max}\cdot k_x\cdot k_l\cdot k_w. \tag{33}$$

Substituting (31) and (33) into (17), the expression of the turns-coefficient k_N can be obtained

$$k_N = \frac{\psi_{m-\Sigma}}{N_S\cdot\psi_{m-1}} = \frac{\sum_{i=1}^{N_S}k_{l-i}\cdot k_{w-i}}{N_S\cdot k_l\cdot k_w}. \tag{34}$$

According to (29), (30), and (34), the value of the turns-coefficient k_N is related to N_S, *dd*, l_{coil} and w_{coil}. When the coil size and wire diameter are determined, the value of k_N at different turns can be quickly obtained by MATLAB.

During the receiver design process, $k_N \sim N_S$ curves can be quickly drawn by MATLAB. Fig. 12 shows $k_N \sim N_S$ curves of the receiver coils with different sizes. The $k_N \sim N_S$ curve can be used to obtain k_N at different turns, and then the number of turns required to meet the output power can be calculated.

D. Distance-Coefficient

Distance-coefficient k_d is used to describe the functional relationship between the mutual inductance and the center distance between the receiver coils. For a structure where the center distance d_c is equal to the pole pitch τ [as shown in Fig. 6 (a)], the total mutual flux linkage passing through the receiver coils (denoted as ψ_{mq}) is equal to the product of the number of coils q and the flux linkage passing through a single coil, and it can be expressed as follows:

$$\psi_{mq} = q\cdot\psi_m. \tag{35}$$

While, for a receiver structure where the center distance d_c is not equal to the pole pitch τ [as shown in Fig. 6(b)], the relationship between the positon of the receiver and the flux linkage passing through each receiver coil is shown in Fig. 7. As shown in the figure, the flux linkages passing through the receiver coils can be expressed as follows:

$$\begin{cases}\psi_{m-\text{coil1}} = -\psi_{m-\max}\cdot\cos(\frac{\pi}{\tau}\cdot x - \frac{\pi}{\tau}\cdot d_c) \\ \qquad\qquad = \psi_{m-\max}\cdot\cos(\frac{\pi}{\tau}\cdot x + \alpha) \\ \psi_{m-\text{coil2}} = \psi_{m-\max}\cdot\cos(\frac{\pi}{\tau}\cdot x) \\ \psi_{m-\text{coil3}} = -\psi_{m-\max}\cdot\cos(\frac{\pi}{\tau}\cdot x + \frac{\pi}{\tau}\cdot d_c) \\ \qquad\qquad = \psi_{m-\max}\cdot\cos(\frac{\pi}{\tau}\cdot x - \alpha)\end{cases} \tag{36}$$

where

$$\alpha = \frac{\tau - d_c}{\tau}\cdot\pi. \tag{37}$$

According to (36) and (37), the mutual flux linkages passing through each coil have the same amplitude, but a phase difference of α along the driving direction (*x*-axis direction).

According to (37), α is only determined by d_c and τ, and it is independent of the receiver's position. During the driving process of the receiver, only the position of the receiver x varies, whereas d_c and τ remain unchanged. Therefore, the phase difference between the flux linkages passing through the receiver coils is always fixed at a constant value.

At this time, ψ_{mq} is equal to the phasor sum of the mutual flux linkages passing through each coil ($\psi_{m\text{-coil1}}$, $\psi_{m\text{-coil2}}$, and $\psi_{m\text{-coil3}}$). Fig. 13 shows the phasor diagram of the mutual flux linkage passing through the receiver coils when $q = 3$.

To clearly describe the relationship between ψ_{mq} and the mutual flux linkage passing through each receiver coil, the circumscribed circle of the regular polygon composed of $\psi_{m\text{-coil1}}$, $\psi_{m\text{-coil2}}$, and $\psi_{m\text{-coil3}}$ is drawn in Fig. 13. The circle center is *O* and the radius is *R*. As shown in the figure, the phasors of the mutual flux linkage passing through the adjacent two coils have a phase difference of α. And each phasor has a central angle of α as well. According to the geometric relationship, the radius *R* of the circumscribed circle satisfies

$$R = \frac{\psi_{m-\max}}{2\cdot\sin\frac{\alpha}{2}}. \tag{38}$$

Moreover, the central angle of ψ_{mq} is $q\alpha$; thus, the magnitude of ψ_{mq} can be expressed as

$$\psi_{mq} = 2R\cdot\sin\left(\frac{q\cdot\alpha}{2}\right) = q\cdot\psi_{\max}\cdot\frac{\sin\frac{q\cdot\alpha}{2}}{q\cdot\sin\frac{\alpha}{2}}. \tag{39}$$

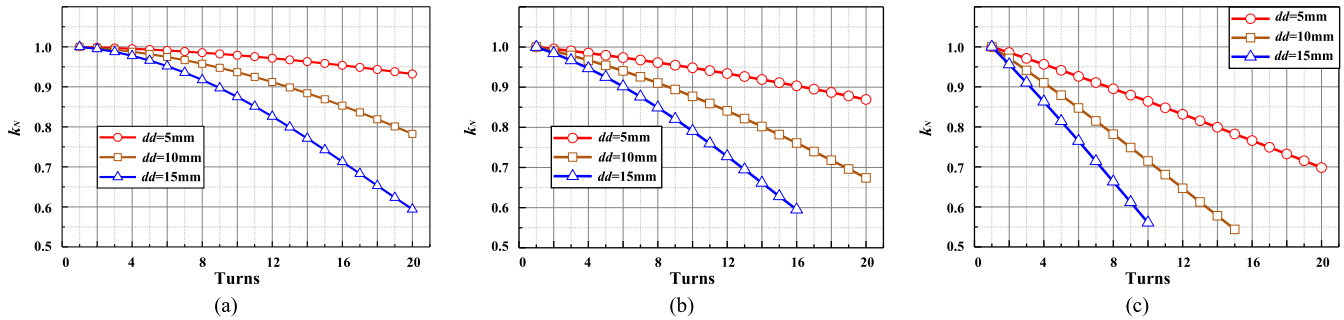

Fig. 12. k_N~N_S curves when: (a) $l_{\text{coil}} = 600$ mm and $w_{\text{coil}} = 800$ mm; (b) $l_{\text{coil}} = 500$ mm and $w_{\text{coil}} = 800$ mm; (c) $l_{\text{coil}} = 300$ mm and $w_{\text{coil}} = 800$ mm.

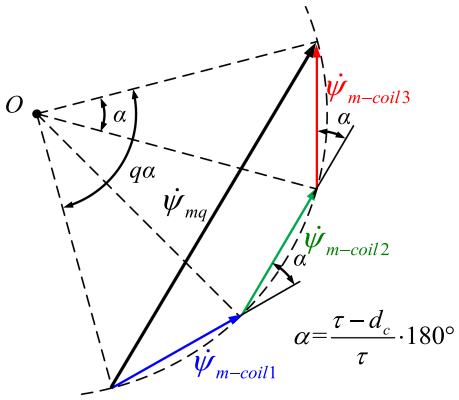

Fig. 13. Phasor diagram of the mutual flux linkage passing through the receiver coils when $q = 3$.

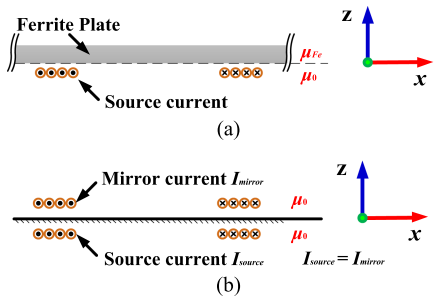

Fig. 14. Working principle of the magnetic mirror model. (a) Actual model of the receiver coil with a plate receiver core. (b) Equivalent magnetic mirror model.

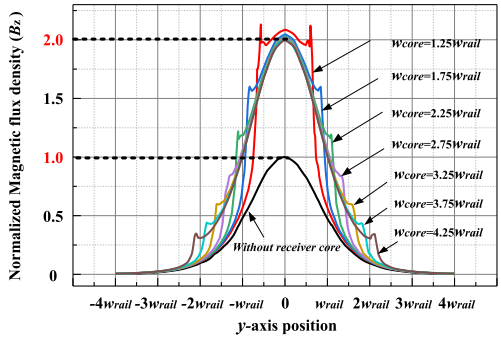

Fig. 15. Distribution of B_z on the straight line $x = 0$ versus the width of receiver core. (The length of the receiver core satisfies: $l_{\text{core}} = 2.25\tau$).

In summary, distance-coefficient k_d can be obtained by the ratio of (39) and (35), and its expression is as follows:

$$k_d = \frac{\sin\frac{q\cdot\alpha}{2}}{q\cdot\sin\frac{\alpha}{2}}. \tag{40}$$

It is worth noting that the distance-coefficient is only suitable for the case where the structures of the multiple receiver coils are the same. When the structures of multiple coils are different, the total mutual flux linkage ψ_{mq} should be calculated with the help of the flux phasor diagram.

E. Core-Coefficient

Magnetic mirror model for a plate core with infinite permeability and an infinite size is commonly used to calculate the magnetic field distribution [29], [30]. Based on the magnetic mirror mode, the actual model of the receiver coil with a plate receiver core shown in Fig. 14(a) can be replaced by the equivalent model shown in Fig. 14(b), where the mirror current and the source current are symmetrically distributed on the surface of the receiver core.

When the size and the permeability of the plate core are infinite, the amplitudes of the source current and the mirror current are equal [29]. However, in engineering applications, due to the limited size of the receiver core, the amplitude of the mirror current is slightly less than the source current. As a result, the amplification factor of the mutual inductance is less than 2. Therefore, the core-coefficient k_c satisfies that $k_c \leq 2$.

1) Effect of the Width of the Plate Core on k_c: In this article, the relationship between k_c and the size of the receiver core is studied by finite-element method (FEM). Simulation results show that the width of plate core does not affect the distribution of B_z along the x-axis, but mainly affects the distribution of B_z along the y-axis. Fig. 15 shows the distribution of B_z on the straight line ($x = 0$) when the width of the core is varying.

It can be known from Fig. 15 that:

1) When the width of the receiver core (denoted as w_{core}) is approximately equal to the width of the power supply rail (denoted as w_{rail}), the distribution of B_z in the region

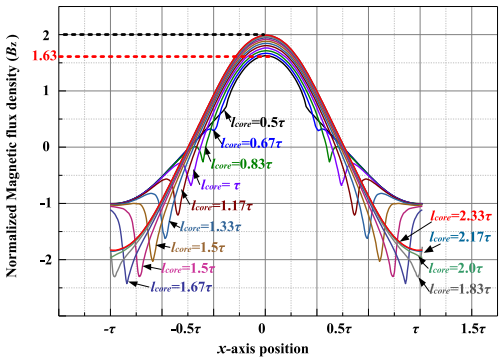

Fig. 16. Distribution of B_z on the straight line $y = 0$ versus the length of receiver core. (The width of the receiver core satisfies: $w_{\rm core} = 4\tau/3$).

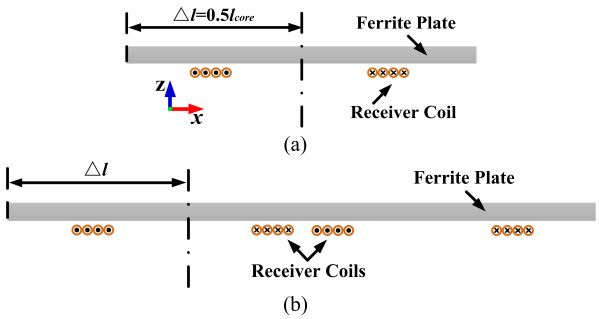

Fig. 17. Structure diagrams of the receiver. (a) With a single-receiver coil. (b) With multireceiver coils.

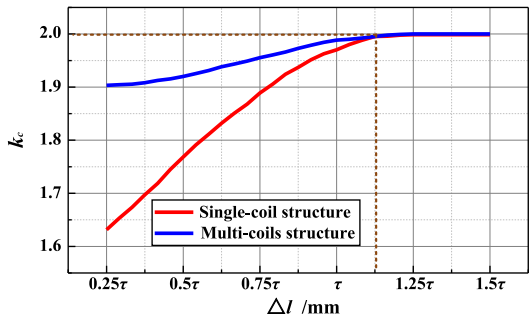

Fig. 18. Core-coefficient k_c versus Δl.

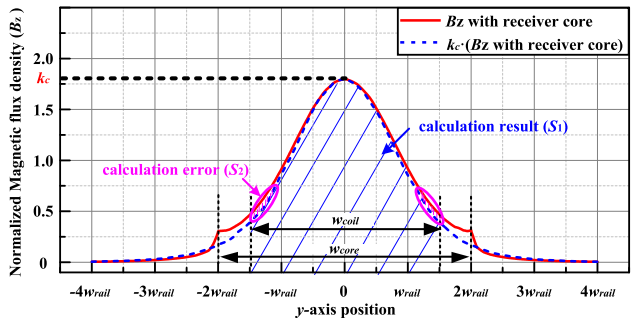

Fig. 19. Simulation result and fitting result of the distribution of B_z along the y-axis when a plate receiver core is used.

below the plate core is distorted due to the core's end effect. As a result, the core-coefficient k_c is greater than 2.

2) When $w_{\rm core} \geq 1.75 w_{\rm rail}$, the width of the plate core has no effect on the distribution of B_z in the region directly below the core, while it only affects the distribution of B_z in the region below the edge of the core and the region beyond the core. At this time, k_c remains constant and is not affected by $w_{\rm core}$.

Since the widths of power supply rails with alternately arranged poles are narrow (4–20 mm) [26], [27], [31], [32], $w_{\rm core}$ is generally several times more than $w_{\rm rail}$. Therefore, the effect of plate core's width on k_c can be usually ignored.

2) Effect of the Length of the Plate Core on k_c: Similarly, the effect of the core length (denoted as $l_{\rm core}$) on k_c is also studied by FEM. The simulation results show that $l_{\rm core}$ does not affect the distribution of B_z along the y-axis, but affects the amplitude of B_z and its distribution along the x-axis. Fig. 16 shows the distribution of B_z on the straight line ($y = 0$) when the length of core is varying.

The simulation result shows that k_c is mainly affected by $l_{\rm core}$, and will increase as $l_{\rm core}$ increases. When $l_{\rm core} \geq 2.25\tau$, the core-coefficient k_c is equal to 2 and no longer changed with $l_{\rm core}$.

For the receiver with single receiver coil [see Fig. 17(a)], the axis of the coil coincides with the axis of the receiver core, and the distance from the ends of the core to the coil axis (denoted as Δl) satisfies that: $\Delta l = 0.5 l_{\rm core}$. In this case, k_c is independent of the relative position of the plate core and the receiver coil, and it is only affected by $l_{\rm core}$.

While, for the receiver with multireceiver coils [shown in Fig. 17(b)], the axis of the receiver coil and the axis of the receiver core no longer coincide. In this case, k_c is not only affected by $l_{\rm core}$, but also affected by the relative position of the plate core and the receiver coil. As shown in Fig. 17(b), the distance from one end of the plate core to the coil axis is much longer than the length of the receiver coil. Therefore, k_c is then determined by the shorter distance from the coil axis to the core end [Δl shown in Fig. 17(b)]. By FME, Fig. 18 shows the relationships between k_c and Δl in the single-coil receiver structure and the multi-coils receiver structure, respectively. According to the receiver structure and the length of Δl, core-coefficient k_c can be obtained from Fig. 18.

3) Adaptability of k_c: As shown in Fig. 3, in the region below the edge of the receiver core, B_z has a small distortion due to the end effect. When the size of the receiver coil is close to that of the plate receiver core, due to the distortion of B_z, the actual mutual flux linkage passing through the receiver coil is not exactly equal to that calculated by the core-coefficient k_c, which results in a calculation error. Therefore, the adaptability of k_c is discussed later.

The distributions of B_z along the y-axis (lateral direction) is shown in Fig. 19. The red solid curve in the figure is the simulation result of B_z, while the blue dotted curve is the fitting result. Due to the end effect, the two curves do not coincide completely in the region below the edge of the receiver core.

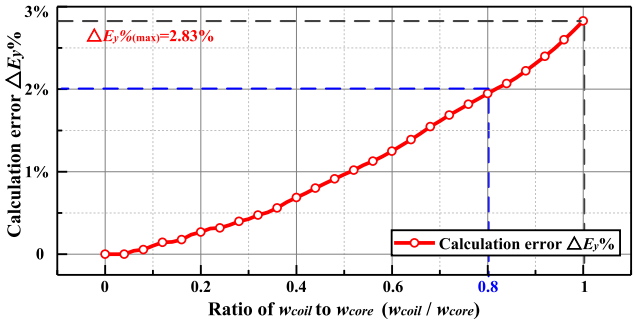

Fig. 20. Calculation error $\Delta E_y\%$ versus the ratio of $w_{\rm coil}$ to $w_{\rm core}$.

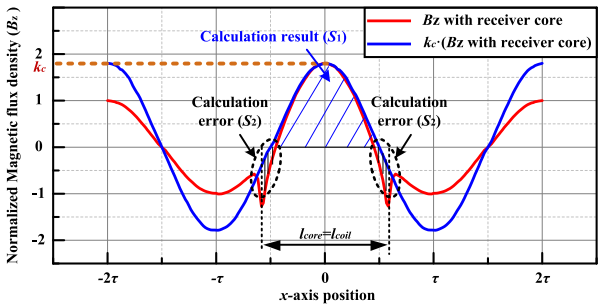

Fig. 21. Simulation result and fitting result of the distribution of B_z along the x-axis when a plate receiver core is used.

The blue shaded area (S_1) is the integral of fitting B_z (fitted by the core-coefficient k_c) along the y-axis. According to (12), mutual flux linkage is proportional to the integral of B_z along the y-axis direction. Therefore, the area of S_1 is proportional to the calculation mutual inductance. And the red shaded area (S_2) in Fig. 19 is the calculation error.

Therefore, the calculation error along the y-axis direction (denoted as $\Delta E_y\%$) can be expressed as follows:

$$\Delta E_y\% = \left(1 - \frac{S_1}{S_1 + 2S_2}\right) \cdot 100\% = \left(\frac{2S_2}{S_1 + 2S_2}\right)\%. \tag{41}$$

It can be seen from Fig. 19 that $\Delta E_y\%$ is affected by the ratio of the receiver coil width (denoted as $w_{\rm coil}$) to the receiver core width (denoted as $w_{\rm core}$). The variation of $\Delta E_y\%$ with the ratio of $w_{\rm coil}$ to $w_{\rm core}$ is shown in Fig. 20.

When $w_{\rm core}$ is fixed, the calculation error $\Delta E_y\%$ gradually increases as $w_{\rm coil}$ increases. When $w_{\rm coil} = w_{\rm core}$, $\Delta E_y\%$ reaches the maximum value of 2.83%.

The width of the plate receiver core will also affect the calculation error $\Delta E_y\%$. For the receiver cores with different widths, calculation results show that calculation error $\Delta E_y\%$ is always less than 3% when $w_{\rm coil}$ and $w_{\rm core}$ satisfy that $w_{\rm core} \geq 1.75 w_{\rm rail}$ and $w_{\rm coil} \leq w_{\rm core}$. Since the calculation processes of $\Delta E_y\%$ with different core widths are similar to that mentioned above, it is not discussed here.

In addition, due to the limited length of the receiver core, the distortion of B_z will also occur along the x-axis direction (driving direction). When $l_{\rm core} = 7\tau/6$, the distributions of B_z along the x-axis direction is shown in Fig. 21.

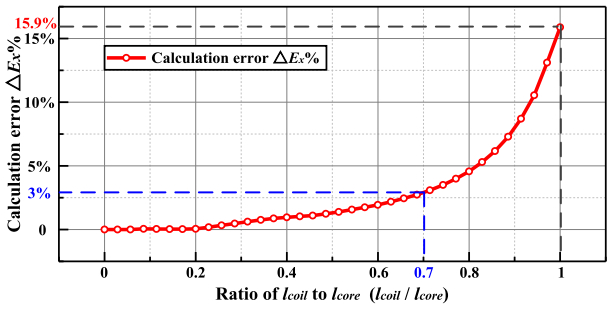

Fig. 22. Calculation error $\Delta E_x\%$ versus the ratio of $l_{\rm coil}$ to $l_{\rm core}$.

Due to the end effect, the curves of simulation result and fitting result do not coincide completely in the region below the edge of the receiver core. As a result, when the length of the receiver coil $l_{\rm coil}$ is close to the length of the plate receiver core $l_{\rm core}$, the actual mutual flux linkage passing through the receiver coil is not exactly equal to the mutual flux linkage calculated by the core-coefficient k_c. At this time, the red shaded area (S_2) shown in Fig. 21 is the calculation error (denoted as $\Delta E_x\%$).

The variation of $\Delta E_x\%$ with the ratio of $l_{\rm coil}$ to $l_{\rm core}$ is shown in Fig. 22.

As shown in the figure, when $l_{\rm core}$ is fixed, the calculation error of the proposed method $\Delta E_x\%$ gradually increases as $l_{\rm coil}$ increases. When $l_{\rm coil} = l_{\rm core}$, the calculation error $\Delta E_x\%$ reaches the maximum value of 15.9%. When $l_{\rm coil} \leq 0.7 l_{\rm core}$, $\Delta E_x\%$ is less than 3%. The comparison between Figs. 20 and 22 shows that the calculation error caused by the distortion of B_z along the x-axis is obviously larger than that along the y-axis.

For the receiver cores with different lengths, calculation results show that the calculation error $E_x\%$ is always less than 3% when $l_{\rm coil}$ and $l_{\rm core}$ satisfy that $l_{\rm coil} \leq 0.7 l_{\rm core}$.

In conclusion, when the mutual inductance of the magnetic coupler with receiver core is calculated by the core-coefficient k_c, the size of the receiver coil and the size of the plate receiver core should satisfy the constraint that $l_{\rm coil} \leq 0.7 l_{\rm core}$ and $w_{\rm coil} \leq w_{\rm core}$. At this time, the calculation error can meet the error requirement in engineering. In future research, the functional relationship between the size of the receiver core and the distortion of B_z will be analyzed and a correction coefficient will be proposed to reduce the calculation error and improve the adaptability the proposed calculation method.

IV. Experimental Verification

A. Prototype

To verify the correctness and the accuracy of the proposed calculation-coefficients and the mutual inductance calculation method, an experiment prototype shown in Fig. 23(a) was built. In the prototype, the air gap h was 21 cm, and the transmitter adopted an N-type power supply rail with a total length of 4.8 m. The structure parameters of the power supply rail are given in Table I. In addition, several receiver coils shown in Fig. 23(b) were built. All the coils were wound by Litz wire with 3000 strands and 2 mm wire diameter, the number of turns were 5.

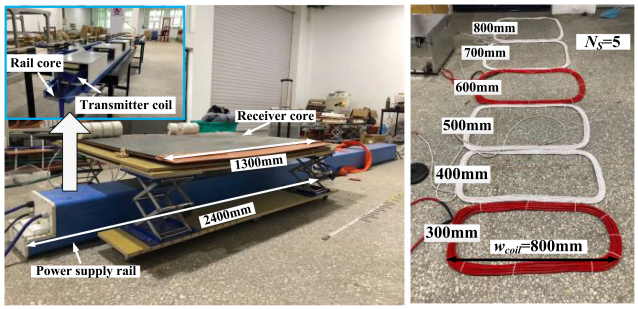

Fig. 23. Prototype. (a) Overview. (b) Receiver coils of different sizes.

TABLE I
PARAMETERS OF THE N-TYPE POWER SUPPLY RAIL

Parameter	Symbol	Value	Unit
Pole pitch	τ	600	mm
Pole shoe length	l_b	300	mm
Pole shoe width	w_b	200	mm
Pole shoe thickness	t_b	10	mm
Pole yoke width	w_j	100	mm
Pole yoke thickness	t_j	30	mm
Pole body length	l_m	100	mm
Pole body thickness	t_m	20	mm
Pole body height	h_m	100	mm
Number of transmitter coils turns	N_P	4	-
Current in transmitter coils(rms)	I_p	80	A

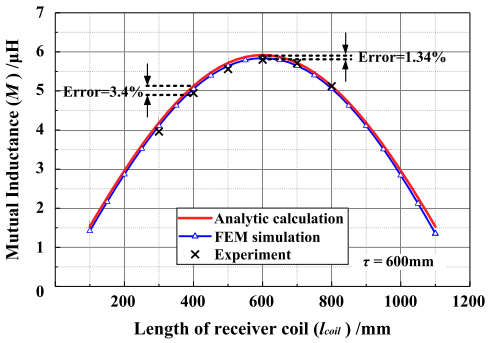

Fig. 24. Mutual inductance versus the length of the receiver coil (without receiver core).

B. Verification of Calculation Coefficients

1) Length-Coefficient: To verify the correctness of length-coefficient k_l, a finite element model was established for simulation, and several receiver coils were wound for experiment. The widths of the coils were 800 mm, the lengths of the coils ranged from 300 to 800 mm, and the wire diameter was 2 mm.

Fig. 24 shows the simulation result, experiment result and calculation result of the mutual inductance when the length of the receiver coil length varies.

As shown in the figure, the mutual inductance varied sinusoidally with the length of the receiver coil, and reaches the maximum when the length of the coil is equal to the pole pitch. The maximum error between the calculation result and the simulation result was 1.34%, and the maximum error between the calculation result and the experiment result was 3.4%. The experiment result was consistent with the theoretical analysis, which verified the correctness and accuracy of the proposed length-coefficient.

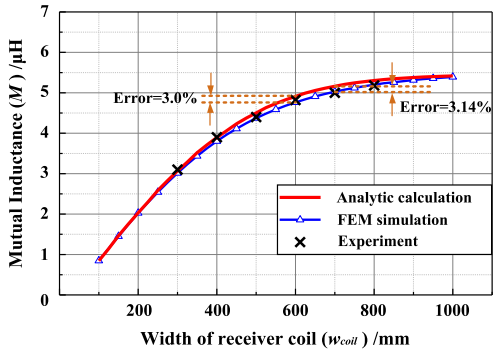

Fig. 25. Mutual inductance versus the width of the receiver coil (without receiver core).

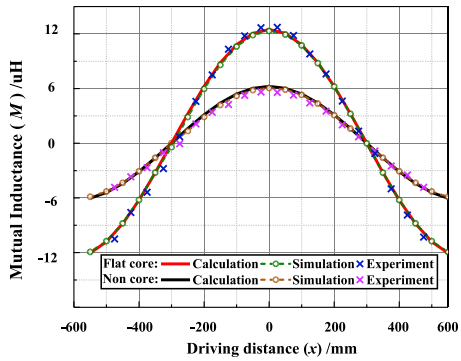

Fig. 26. Mutual inductance versus driving distance x with/without receiver core.

2) Width-Coefficient: To verify the correctness of width-coefficient k_w, a simulation model was established and several receiver coils were wound. In both the simulation and experiment models, the lengths of the coils were 800 mm, the widths of the coils ranged from 300 to 800 mm, and the wire diameter was 2 mm.

Fig. 25 shows the simulation result, experiment result and calculation result of mutual inductance when the width of the receiver coil length varies.

As the width of the receiver coil varied, the maximum errors between the calculation result and the simulation result was 3.0%, and the maximum error between the calculation result and the experiment result was 3.14%. The results verified the correctness and accuracy of the proposed width-coefficient.

3) Core-Coefficient and Position-Coefficient: To verify the correctness of core-coefficient k_c and position-coefficient k_x, when the receiver moved along the driving direction, the mutual inductance with or without plate receiver core was obtained by simulation and measurement, respectively. In the prototype and the simulation model, the receiver adopted single-coil structure. The parameters of the receiver coil were $l_{\mathrm{coil}} = 600$ mm, $w_{\mathrm{coil}} = 800$ mm, $dd = 2$ mm, and $N_S = 5$, and the structure parameters of the plate receiver core were: 1300 mm $\times$ 800 mm $\times$ 10 mm.

Fig. 26 shows the simulation result, experiment result, and calculation result.

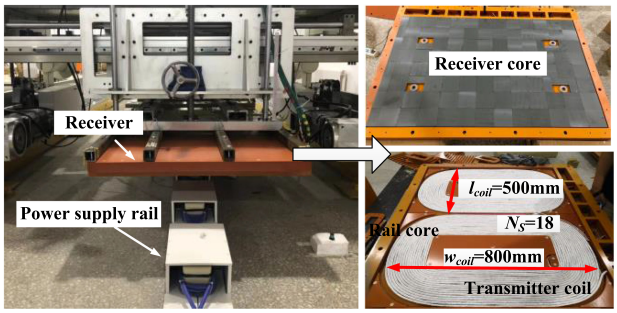

Fig. 27. Engineering DWC prototype.

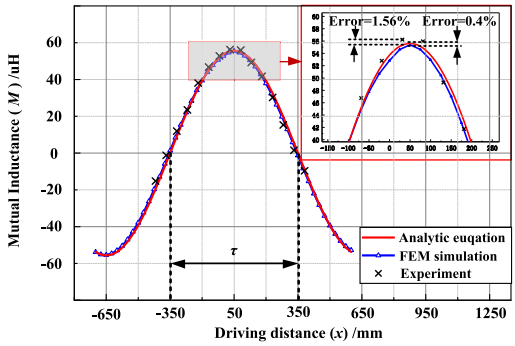

Fig. 28. Calculation, simulation, and measured results of the mutual inductance versus driving distance x.

It can be seen from the earlier figure that results are as follows.

1) Whether the plate receiver core existed or not, $M\sim x$ curves were all sine functions, which verified the correctness of the position-coefficient k_x.
2) Along the driving direction, the mutual inductance with a plate core is twice as much as that without receiver core, which verified the correctness of the core-coefficient k_c.
3) The calculation result of the mutual inductance was basically the same as the simulation and experiment results, which verified the accuracy of the position-coefficient and the core-coefficient.

Based on the prototype shown in Fig. 23, the correctness and accuracy of length-coefficient, width-coefficient, position–coefficient, and core-coefficient were all verified. However, since the coils' number and the coil's number of turns in the prototype were not easy to adjust, the correctness of distance-coefficient k_d and turns-coefficient k_N was verified in the following experiments.

C. Verification of the Proposed Calculation Method

To verify the feasibility and the accuracy of the proposed mutual inductance calculation method, another engineering DWC prototype was built for experiments (see Fig. 27).

In this prototype, the air gap and the structure parameters of the power supply rail remained unchanged, while the total length of the power supply rail was changed to 9.6 m. The receiver adopted multi-coils structure, and the receiver coils were composed of two DD coils connected in series. The structure parameters of a single D receiver coil satisfied that $l_{\rm coil} = 500$ mm, $w_{\rm coil} = 800$ mm, $N_S = 18$, and $dd = 10$ mm, and the center distance d_c between the two DD coils was equal to the coil length. The receiver adopted a plate receiver core with a size of 1250 mm $\times$ 800 mm $\times$ 10 mm.

As the receiver moved along the driving direction, the mutual inductance was measured by an impedance analyzer. The comparison of the calculation result with the simulation result and the experiment result was shown in Fig. 28.

For the receiver structure with multicoils, the maximum error between the calculation result and the simulation result was 0.4%, and the maximum error between the calculation result and the experiment result was 1.56%. Both the simulation result and the experiment result verified the correctness of distance-coefficient k_d and turns-coefficient k_N, and also verified the feasibility and the accuracy of the proposed mutual inductance calculation method.

V. Conclusion

A fast and general method to calculate mutual inductance for the EV DWC system is proposed in this article. This method uses calculation-coefficients to describe the functional relationships between mutual inductance and the receiver's parameters, and it can simplify the surface-integral in the conventional analytical method to be the product of the coefficients to reduce the calculation difficulty. In addition, when the proposed method is applied to the design and optimization of the receiver, the problems such as long simulation time and large computer memory consumption in the conventional FEM can also be solved.

Simulation models and prototypes were built, respectively, to verify the proposed mutual inductance calculation method. The maximum error between the calculation result, the simulation result and the experiment result was only 1.56%, which verified the feasibility and the accuracy of the proposed calculation method.

The proposed method cannot only provide a theoretical guidance for the receiver structure design, but also be applied to the fast comparison of different receiver structures and the calculation of the receiver's maximum lateral displacement. In the next article, the specific applications of the proposed calculation methods will be introduced in detail.

References

[1] C. C. Mi, G. Buja, S. Y. Choi, and C. T. Rim, "Modern advances in wireless power transfer systems for roadway powered electric vehicles," *IEEE Trans. Ind. Electron.*, vol. 63, no. 10, pp. 6533–6545, Oct. 2016.

[2] G. Buja, M. Bertoluzzo, and H. K. Dashora, "Lumped track layout design for dynamic wireless charging of electric vehicles," *IEEE Trans. Ind. Electron.*, vol. 63, no. 10, pp. 6631–6640, Oct. 2016.

[3] A. Ahmad, M. S. Alam, and R. Chabaan, "A comprehensive review of wireless charging technologies for electric vehicles," *IEEE Trans. Transp. Electrific.*, vol. 4, no. 1, pp. 38–63, Mar. 2018.

[4] A. F. A. Aziz, M. F. Romlie, and Z. Baharudin, "Review of inductively coupled power transfer for electric vehicle charging," *IET Power Electron.*, vol. 12, pp. 3611–3623, 2019.

[5] J. Shin *et al.*, "Design and implementation of shaped magnetic-resonance-based wireless power transfer system for roadway-powered moving electric vehicles," *IEEE Trans. Ind. Electron.*, vol. 61, no. 3, pp. 1179–1192, Mar. 2014.
[6] R. Tavakoli and Z. Pantic, "Analysis, design, and demonstration of a 25-kW dynamic wireless charging system for roadway electric vehicles," *IEEE J. Emerg. Sel. Topics Power Electron.*, vol. 6, no. 3, pp. 1378–1393, Sep. 2018.
[7] J. H. Kim *et al.*, "Development of 1-MW inductive power transfer system for a high-speed train," *IEEE Trans. Ind. Electron.*, vol. 62, no. 10, pp. 6242–6250, Oct. 2015.
[8] K. Lee and D. Cho, "Analysis of wireless power transfer for adjustable power distribution among multiple receivers," *IEEE Antennas Wireless Propag. Lett.*, vol. 14, pp. 950–953, Jan. 2015.
[9] Z. H. Shi, X. Y. Chen, and Z. C. Qiu, "Modeling of mutual inductance between superconducting pancake coils used in wireless power transfer (WPT) systems," *IEEE Trans. Appl. Supercond.*, vol. 29, no. 2, Mar. 2019, Art. no. 5500904.
[10] X.Zhang, H. Meng, B. Wei, S. Wang, and Q. Yang, "Mutual inductance calculation for coils with misalignment in wireless power transfer," *J. Eng.*, vol. 2019, pp. 1041–1044, 2019.
[11] S. R. Khan, S. K. Pavuluri, and M. P. Y. Desmulliez, "Accurate modeling of coil inductance for near-field wireless power transfer," *IEEE Trans. Microw. Theory Techn.*, vol. 66, no. 9, pp. 4158–4169, Sep. 2018.
[12] F. Liu, Y. Yang, D. Jiang, X. Ruan, and X. Chen, "Modeling and optimization of magnetically coupled resonant wireless power transfer system with varying spatial scales," *IEEE Trans. Power Electron.*, vol. 32, no. 4 pp. 3240–3250, Apr. 2017.
[13] S. Raju, R. Wu, M. Chan, and C. P. Yue, "Modeling of mutual coupling between planar inductors in wireless power applications," *IEEE Trans. Power Electron.*, vol. 29, no. 1, pp. 481–490, Jan. 2014.
[14] W. G. Hurley, M. C. Duffy, J. Zhang, I. Lope, B. Kunz, and W. H. Wölfle, "A unified approach to the calculation of self- and mutual-inductance for coaxial coils in air," *IEEE Trans. Power Electron.*, vol. 30, no. 11, pp. 6155–6162, Nov. 2015.
[15] B. K. Kushwaha, G. Rituraj, and P. Kumar, "3-D analytical model for computation of mutual inductance for different misalignments with shielding in wireless power transfer system," *IEEE Trans. Transp. Electrific.*, vol. 3, no. 2, pp. 332–342, Jun. 2017.
[16] Y. Cheng and Y. Shu, "A new analytical calculation of the mutual inductance of the coaxial spiral rectangular coils," *IEEE Trans. Magn.*, vol. 50, no. 4, Apr. 2014, Art no. 7026806.
[17] S. H. Lee, B. S. Lee, J. H. Lee, C. B. Park, and J. H. Kim, "A new design methodology for a 300 kW, low flux density, large air-gap, on-line wireless power transfer system," *IEEE Trans. Ind. Appl.*, vol. 52, no. 5, pp. 4234–4242, Sep.-Oct. 2016.
[18] H. Li, Y. Liu, K. Zhou, Z. He, W. Li, and R. Mai, "Uniform power IPT system with three-phase transmitter and bipolar receiver for dynamic charging," *IEEE Trans. Power Electron.*, vol. 34, no. 3, pp. 2013–2017, Mar. 2019.
[19] Z. Wang *et al.*, "A novel magnetic coupling mechanism for dynamic wireless charging system for electric vehicles," *IEEE Trans. Veh. Technol.*, vol. 67, no. 1, pp. 124–133, Jan. 2018.
[20] S. Cui, B. Song, X. Gao, and S. Dong, "A narrow-width three phase magnetic coupling mechanism with constant output power for electric vehicles dynamic wireless charging," in *Proc. IEEE PELS Workshop Emerg. Technol.: Wireless Power Transfer*, 2018, pp. 1–6.
[21] M. G. S. Pearce, G. A. Covic, and J. T. Boys, "Robust ferrite-less double d topology for roadway IPT applications," *IEEE Trans. Power Electron.*, vol. 34, no. 7, pp. 6062–6075, Jul. 2019.
[22] S. B. Lee, S. Ahn, and I. G. Jang, "Simulation-based feasibility study on the wireless charging railway system with a ferriteless primary module," *IEEE Trans. Veh. Technol.*, vol. 66, no. 2, pp. 1004–1010, Feb. 2017.
[23] S. Cui, Z. Wang, S. Han, C. Zhu, and C. C. Chan, "Analysis and design of multiphase receiver with reduction of output fluctuation for EV dynamic wireless charging system," *IEEE Trans. Power Electron.*, vol. 34, no. 5, pp. 4112–4124, May 2019.
[24] L. Ming and K. D. T. Ngo, "A fast method to optimize efficiency and stray magnetic field for inductive-power-transfer coils using lumped-loops model," *IEEE Trans. Power Electron.*, vol. 33, no. 4, pp. 3065–3075, Apr. 2018.
[25] Z. Wang, S. Cui, B. Song, S. Han, and C. Zhu, "Comprehensive optimisation and comparison of multiphase receiver for dynamic wireless charging system," *IET Power Electron.*, vol. 12, pp. 2475–2484, 2019.
[26] J. Huh, S. W. Lee, W. Y. Lee, G. H. Cho, and C. T. Rim, "Narrow-width inductive power transfer system for online electrical vehicles," *IEEE Trans. Power Electron.*, vol. 26, no. 12, pp. 3666–3679, Dec. 2011.
[27] S. Y. Choi, S. Y. Jeong, B. W. Gu, G. C. Lim, and C. T. Rim, "Ultraslim S-type power supply rails for roadway-powered electric vehicles generalized models on self-decoupled dual pick-up coils for a large lateral tolerance," *IEEE Trans. Power Electron.*, vol. 30, no. 11, pp. 6456–6468, Nov. 2015.
[28] F. Musavi and W. Eberle, "Overview of wireless power transfer technologies for electric vehicle battery charging," *IET Power Electronics*, vol. 7, pp. 60–66, 2014.
[29] W. Y. Lee *et al.*, "Finite-width magnetic mirror models of mono and dual coils for wireless electric vehicles," *IEEE Trans. Power Electron.*, vol. 28, no. 3, pp. 1413–1428, Mar. 2013.
[30] M. Curti, J. J. H. Paulides, and E. A. Lomonova, "An overview of analytical methods for magnetic field computation," in *Proc. 10th Int. Conf. Ecological Veh. Renew. Energies*, 2015, pp. 1–7.
[31] C. Park, S. Lee, S. Y. Jeong, G. Cho, and C. T. Rim, "Uniform power I-type inductive power transfer system with dq-power supply rails for on-line electric vehicles," *IEEE Trans. Power Electron.*, vol. 30, no. 11, pp. 6446–6455, Nov. 2015.
[32] Y. C. Su, S. Y. Jeong, E. S. Lee, B. W. Gu, S. W. Lee, and C. T. Rim, "Generalized models on self-decoupled dual pick-up coils for large lateral tolerance," *IEEE Trans. Power Electron.*, vol. 30, no. 11, pp. 6434–6445, Nov. 2015.

Beibei Song was born in Henan Province, China, in 1993. He received the B.S. and M.S. degrees in electrical engineering in 2016 and 2018, respectively, from the Harbin Institute of Technology, Harbin, China, where is currently working toward Ph.D. degree.

His research interests include wireless power transfer and dynamic wireless charging for electric vehicles.

Shumei Cui was born in Heilongjiang, China, on November 22, 1964. She received the Ph.D. degree in electrical engineering from the Harbin Institute of Technology (HIT), Harbin, China, in 1998.

She has been a Professor with the Department of Electrical Engineering, HIT. Her research interests include the design and control of micro and special electric machines, electric drive system of electric vehicles, control and simulation of hybrid electric vehicles, and intelligent test and fault diagnostics of electric machines.

Dr. Cui is currently the Vice Director Member of the Micro and Special Electric Machine Committee and the Chinese Institute of Electronics, and a member of the Electric Vehicle Committee and the National Automotive Standardization Technical Committee.

Yong Li was born in Heilongjiang, China, in 1964. He received the Ph. degree in electrical engineering from the Harbin Institute of Technology, Harbin, China, in 1988.

He is currently a Professor with the Department of electrical engineering, Harbin Institute of Technology. His research interests include PMSMs, special motors and their applications.

Chunbo Zhu (Member, IEEE) received the B.S. and M.S. degrees in electrical engineering and the Ph.D. degree in mechanical engineering from the Harbin Institute of Technology (HIT), Harbin, China, in 1987, 1992, and 2001, respectively.

From 2003 to 2004, he was a Postdoctoral Research Fellow with the PEI Research Center, National University of Ireland, Galway, Ireland. Since 1987, he has been a Lecturer with the Department of Automation Measurement and Control, HIT. He is currently a Full Professor with HIT, where he leads the Laboratory of Wireless Power Transfer and Battery Management Technologies. His current research interests include energy management systems, electric and hybrid electric vehicles, and wireless power transfer technologies.